Title: Reciprocal cybrids reveal how organellar genomes affect plant phenotypes

Authors:

Pádraic J. Flood[1,2,3†*], Tom P.J.M. Theeuwen[1†*], Korbinian Schneeberger[3], Paul Keizer[4], Willem Kruijer[4], Edouard Severing[3], Evangelos Kouklas[1], Jos A. Hageman[4], Raúl Wijfjes[5], Vanesa Calvo-Baltanas[1], Frank F.M. Becker[1], Sabine K. Schnabel[4], Leo Willems[6], Wilco Ligterink[6], Jeroen van Arkel[7], Roland Mumm[7], José M. Gualberto[8], Linda Savage[9], David M. Kramer[9], Joost J.B. Keurentjes[1], Fred van Eeuwijk[4], Maarten Koornneef[1,3], Jeremy Harbinson[2], Mark G.M. Aarts[1] & Erik Wijnker[1*]

Affiliations:

[1] Laboratory of Genetics, Wageningen University & Research, Wageningen, The Netherlands.

[2] Horticulture and Product Physiology, Wageningen University & Research, Wageningen, The Netherlands.

[3] Department of Plant Developmental Biology, Max Planck Institute for Plant Breeding Research, Cologne, Germany.

[4] Biometris, Wageningen University & Research, Wageningen, The Netherlands.

[5] Bioinformatics Group, Wageningen, The Netherlands

[6] Laboratory of Plant Physiology, Wageningen University & Research, Wageningen, The Netherlands.

[7] Bioscience, Wageningen University & Research, Wageningen, The Netherlands

[8] Institut de Biologie Moléculaire des Plantes, CNRS, Université de Strasbourg, Strasbourg, France.

[9] MSU-DOE Plant Research Lab, Michigan State University, East Lansing, USA

[†] These authors contributed equally to this work

* Correspondence to:

P.J. Flood - flood@mpipz.mpg.de

T.P.J.M. Theeuwen - tom.theeuwen@wur.nl

E. Wijnker - erik.wijnker@wur.nl

Introductory paragraph:

Assessing the impact of variation in chloroplast and mitochondrial DNA (collectively termed the plasmotype) on plant phenotypes is challenging due to the difficulty in separating their effect from nuclear derived variation (the nucleotype). Haploid inducer lines can be used as efficient plasmotype donors to generate new plasmotype-nucleotype combinations (cybrids)(Ravi et al., 2014). We generated a panel comprising all possible cybrids of seven *Arabidopsis thaliana* accessions and extensively phenotyped these lines for 1859 phenotypes under stable and fluctuating conditions. We show that natural variation in the plasmotype results in additive as well as epistatic effects across all phenotypic categories. Plasmotypes which induce more additive phenotypic changes also cause more significant epistatic effects, suggesting a possible common basis for both additive and epistatic effects. On average epistatic interactions explained twice as much of the variance in phenotypes as additive plasmotype effects. The impact of plasmotypic variation was also more pronounced under fluctuating and stressful environmental conditions. Thus, the phenotypic impact of variation in plasmotypes is the outcome of multilevel Nucleotype X Plasmotype X Environment interactions and, as such, the plasmotype is likely to serve as a reservoir of variation which is only exposed under certain conditions. The production of cybrids using haploid inducers is a quick and precise method for assessing the phenotypic effects of natural variation in organellar genomes. It will facilitate efficient screening of unique nucleotype-plasmotype combinations to both improve our understanding of natural variation in nucleotype plasmotype interactions and identify favourable combinations to improve plant performance.

Chloroplasts and mitochondria play essential roles in metabolism, cellular homeostasis and environmental sensing (Petrillo et al., 2014; Chan et al., 2016). Their genomes contain only a limited set of genes whose functioning requires tight coordination with the nucleus through signaling pathways that modulate nuclear and organellar gene expression (Petrillo et al., 2014; Kleine and Leister, 2016). Plasmotype variation can be strongly additive, such as in the case of chloroplast encoded herbicide tolerance (Flood et al., 2016), or can manifest in complex cytonuclear interactions as non-additive, non-linear effects (epistasis), such as found for secondary metabolites (Joseph et al., 2013). The phenotypic consequences of epistasis can be detected when a plasmotype causes phenotypic effects in combination with some, but not all nuclear backgrounds. Recent studies suggest that cytonuclear epistasis is the main route through which variation in the plasmotype is expressed (Zeyl et al., 2005;

60 Montooth et al., 2010; Joseph et al., 2013; Joseph et al., 2013; Tang et al., 2014; Roux et al., 2016;
61 Mossman et al., 2019) and that additive effects are both rare and of small effect.

62 Plasmotypic variation is relevant from an agricultural as well as evolutionary perspective
63 (Levings, 1990; Bock et al., 2014; Dobler et al., 2014), but to understand or utilize it, it is necessary to
64 separate nuclear from mitochondrial and chloroplastic effects. Reciprocal-cross designs, where
65 nucleotypes segregate in different plasmotypic backgrounds, have been used to identify plasmotype-
66 specific quantitative trait loci (Joseph et al., 2013; Tang et al., 2014), but are limited to just two
67 plasmotypes. A larger number of plasmotypes can be studied using backcross designs where
68 plasmotypes are introgressed into different nuclear backgrounds (Dowling et al., 2007; Sambatti et al.,
69 2008; Miclaus et al., 2016; Roux et al., 2016), but backcross approaches are lengthy and any undetected
70 nuclear introgressions may confound the results.

71 To precisely and rapidly address the contribution of organellar variation to plant phenotypes, we
72 explored the use of a haploid inducer line available in *Arabidopsis* (*GFP-tailswap*) (Ravi and Chan, 2010;
73 Ravi et al., 2014). When pollinated with a wild-type plant, the *GFP-tailswap* nuclear genome is lost from
74 the zygote through uniparental genome elimination. This generates haploid cybrid offspring with a
75 paternally derived nuclear genome and maternally (*GFP-tailswap*) derived mitochondria and
76 chloroplasts (Fig. 1). These haploid plants produce stable diploid (doubled haploid) offspring following
77 genome duplication or restitutional meiosis (Ravi and Chan, 2010). We set out to test the use of this
78 approach to investigate how plasmotypic variation affects plant phenotypes and to what extent this
79 variation manifests itself as additive variation or as cytonuclear epistasis.

80 Seven different *Arabidopsis* accessions were selected for our experiment: six that represent a
81 snapshot of natural variation (Bur, C24, Col-0, L*er*-0. Sha, WS-4) and Ely, an accession with a large-
82 effect mutation in the chloroplast-encoded *PsbA* gene (El-Lithy et al., 2005). This mutation results in
83 reduced photosystem II efficiency (El-Lithy et al., 2005; Flood et al., 2014) and was included to evaluate
84 the consequence of a strong plasmotype effect in our test-panel. We first generated haploid inducers
85 for all seven plasmotypes (Fig. 1A) and then used each inducer to generate cybrid offspring for all seven
86 nucleotypes (Fig. 1 B and C). Cybrid genotypes will henceforth be denoted as nucleotype^{plasmotype} (i.e.
87 Ely^{Bur} denotes a cybrid with Ely nucleus and Bur plasmotype). Wild-type nucleotype-plasmotype
88 combinations were also regenerated in this way (hereafter referred to as self-cybrids; i.e. Bur^{Bur}, C24^{C24},
89 etc.) to later compare these with their wild-type progenitors. The genotypes of all haploid cybrids were

90 verified by resequencing. This led to the exclusion of Bur^{C24} and Bur^{Bur}, because of the identification of
91 a nucleotypic *de-novo* duplication of 200kb in these two lines, likely derived from a spontaneous
92 duplication in a Bur wild-type progenitor used in creating these cybrids (see Online methods;
93 Supplementary Fig. 1 to 4). With the exception of Ely^{Sha} for which we obtained seeds at a later stage,
94 we obtained doubled haploid seeds from all haploid cybrids resulting in a testpanel of 46 cybrids and 7
95 wildtype progenitors. As with Ely^{Sha}, Bur^{C24} and Bur^{Bur} were subsequently recreated, and the complete
96 panel will be submitted to NASC. To visualize the genetic variation between lines within our panel we
97 generated neighbor joining trees for the nuclear, mitochondrial and chloroplast genomes
98 (Supplementary Fig. 5). The nucleotypes were found to be approximately equidistant, while the L*er*, Ely
99 and Col plasmotypes appear to be more closely related to each other than the other plasmotypes.

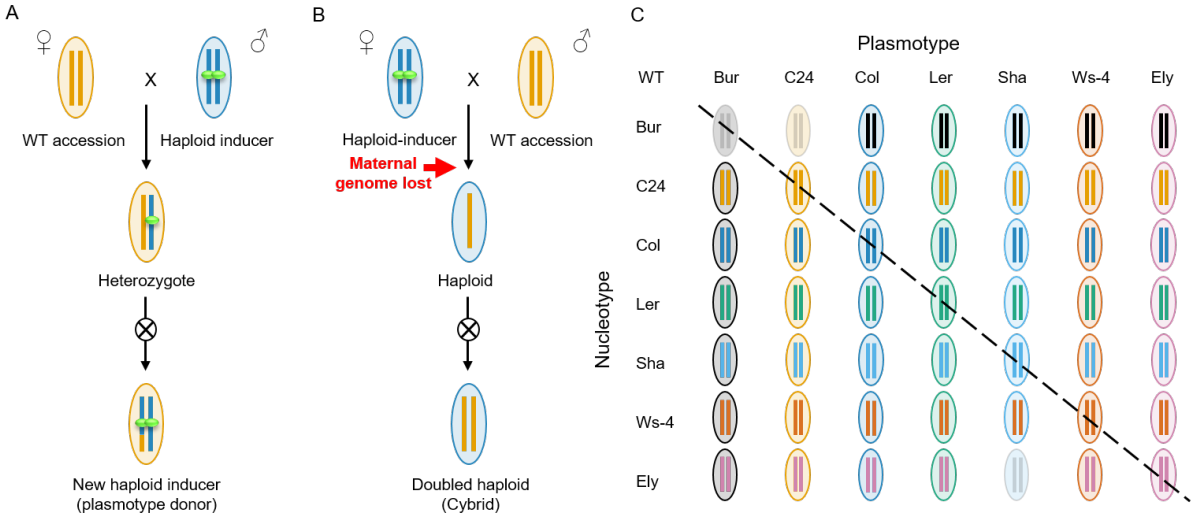

100

101 **Figure 1. Generation of a cybrid test panel.** A) Generation of a new haploid inducer (HI) line with a
102 new plasmotype. The HI expresses a GFP-tagged *CENH3/HRT12* in a *cenh3/htr12* mutant background.
103 A cross of a wild type (female) with a HI (male) results in a hybrid F1. A diploid F1 is selected in which
104 no genome elimination has occurred. Self-fertilization generates an F2 population in the plasmotype of
105 the wild-type mother. From this an F2 plant is selected that is homozygous for the *cenh3/htr12* mutation
106 and carries the *GFP-tailswap* transgene. This F2 plant is a new HI line and can serve as plasmotype
107 donor when used as female in crosses. Vertical bars represent the nucleotype, and the ovals represent
108 the plasmotype. HI centromeres are indicated in green (signifying GFP-tagged CENH3/HTR12 proteins
109 as encoded by the *GFP-tailswap* construct) that cause uniparental genome-elimination. B) HI lines can
110 function as plasmotype donors when used as a female parent. In this case, uniparental genome
111 elimination (red arrow) leads to a haploid offspring plant with the nucleotype of the wild-type (WT) male

112 parent, but the plasmotype of the HI mother. C) Full diallel of all nucleotype-plasmotype combinations
113 for which cybrids were generated. The diagonal line highlights the wild-type (WT) nucleotype-
114 plasmotype combinations that were generated by crossing wild-type plants to plasmotype donors with
115 the plasmotype of the wild type (self-cybrids). Bur^{Bur}, Bur^{C24} and Ely^{Sha} are faded out, as they were not
116 included in the phenotyping experiments, they have been subsequently recreated and the complete set
117 has been submitted to NASC.
118
119 We phenotyped the cybrid panel under constant environmental conditions for absolute and
120 relative growth rate, biomass accumulation, epinastic leaf movement, photosystem II efficiency (Φ_{PSII}),
121 non-photochemical quenching (NPQ), and elements thereof (Φ_{NO}, Φ_{NPQ}, q_E and q_I), a reflectance-based
122 estimate of chlorophyll, flowering time, germination, pollen abortion, and primary metabolites. To
123 simulate more variable conditions that are frequently encountered in the field, we also screened the
124 panel under fluctuating light for all the above-mentioned photosynthesis-related phenotypes and
125 assayed germination rates under osmotic stress and after a controlled deterioration treatment. Counting
126 individual metabolite concentrations and single time points in the time series separately, we collected in
127 total 1859 phenotypes (Supplementary Data 1, Supplementary Table 4). To avoid overrepresentation of
128 highly correlated and non-informative phenotypes we selected a subset of 92 phenotypes (Online
129 methods, Supplementary Table 2) comprising 24 from constant growth conditions, 32 from fluctuating
130 or challenging environmental conditions and 36 primary metabolites for further analysis (Supplementary
131 Fig. 6, Supplementary Table 2).
132 Comparison of six self-cybrids with their genetically identical wild-type progenitors for these 92
133 phenotypes did not reveal significant phenotypic differences (Supplementary Table 1) from which we
134 infer that uniparental genome elimination is a robust method to generate cybrids. To determine the
135 relative contributions of nucleotype, plasmotype, and their interaction to the observed phenotypic
136 variation, we estimated the fraction of the broad sense heritability (H^2; also called repeatability (Falconer
137 and Mackay, 1996)) explained by each. Across the entire panel the average contribution to H^2 of
138 nucleotype, plasmotype and nucleotype-plasmotype interaction was 65.9%, 28.0% and 6.1%
139 respectively (Supplementary Table 2 and 3; Supplementary Data 2). Most of the plasmotype derived
140 additive variation was caused by the Ely plasmotype, arising from the *psbA* mutation. When this
141 plasmotype was excluded from the analysis, the nucleotype, plasmotype and their interaction account

142 for 91.9%, 2.9% and 5.2% of the genetic variation, respectively (Supplementary Table 2 and 3;
143 Supplementary Data 2). So, while nucleotype-derived additive variation is the main genetic determinant
144 of the cybrid phenotype, variation caused by plasmotype additive effects as well as epistatic effects
145 results in substantial phenotypic differences.

146 Next we sought to assess whether there are general patterns in how specific nucleotypes and
147 plasmotypes interact. To this end we first assessed which plasmotype changes result in additive
148 phenotypic changes. Plasmotype replacements involving the Ely plasmotype lead to additive changes
149 in, on average, 50 (out of 92) phenotypes across the 7 nucleotypes (Table 1A). Changes involving the
150 Bur plasmotype lead to on average 10 significant additive effects, 8 of which are photosynthesis-related
151 (Supplementary Data 2). Other plasmotype changes show on average one additive effect, in
152 predominantly non-photosynthetic phenotypes. Comparison of wild-type cytonuclear combinations with
153 all their iso-nuclear cybrid lines also shows that plasmotype changes involving Ely and Bur plasmotypes
154 show the most epistatic effects (on average 43 and 6 respectively) (Table 1B). The number of epistatic
155 effects resulting from the Bur plasmotype range between 0 (Ler^{Ler} vs Ler^{Bur}) to 10 (Sha^{Sha} vs Sha^{Bur}),
156 indicating high variability. Plasmotype changes involving other plasmotypes show more modest
157 numbers of significant epistatic effects that range from 0 to 6. Plasmotypes that result in more additive
158 effects also cause more epistatic effects (Pearson correlation coefficient of 0.99, p-value 1.3e-5)
159 suggesting a possible common cause (Supplementary Fig. 7).
160

161 **Table 1. Significant plasmotype induced effects in 92 phenotypes.** A) Number of observed
162 significant plasmotype additive effects when a specific plasmotype is changed for another plasmotype,
163 regardless of the nucleotype. Note that the replacement of Bur (top row) and Ely plasmotypes (last
164 column) result in most plasmotype additive effects. B) Number of observed significant epistatic effects
165 in phenotypes between wild-type nucleotype-plasmotype combinations and cybrids with different
166 plasmotypes. Rows indicate the number of significant effects when comparing self-cybrids to cybrids
167 with identical nucleotype but non-native plasmotype. Columns indicate specific plasmotype changes.
168 Note that changing the Ely plasmotype for another plasmotype (bottom row and last column) results in
169 many epistatic effects due to the large-effect mutation in the chloroplast-encoded *PsbA* gene of the Ely
170 plasmotype. Similar effects, but of smaller magnitude, result from changing the Bur plasmotype (top row
171 and first column). Posthoc tests were used with Hochberg's p-value correction for panel A and Dunnett's
172 p-value correction (with the wild-type as control) for panel B, α = 0.05. nd = not determined. For
173 underlying p-values and phenotypes see Supplementary Data 2. Yellow cells indicate low number of
174 significant effects; blue cells show higher number of significant effects.

# of significant phenotypes (0 – 55)		Plasmotype						
		XXX^{Bur}	XXX^{C24}	XXX^{Col}	XXX^{Ler}	XXX^{Sha}	XXX$^{Ws\text{-}4}$	XXX^{Ely}
Plasmotype	XXX^{Bur}		12	15	10	15	6	55
	XXX^{C24}			1	0	1	0	50
	XXX^{Col}				2	2	1	50
	XXX^{Ler}					0	1	48
	XXX^{Sha}						2	49
	XXX$^{Ws\text{-}4}$							49
	XXX^{Ely}							

175

# of significant phenotypes (0 – 48)		Plasmotype						
		XXX^{Bur}	XXX^{C24}	XXX^{Col}	XXX^{Ler}	XXX^{Sha}	XXX$^{Ws\text{-}4}$	XXX^{Ely}
wildtype nucleotype-plasmotype combination	Bur wildtype		nd	4	7	9	4	48
	C24^{C24}	4		1	0	3	1	32
	Col^{Col}	5	2		0	1	1	39
	Ler^{Ler}	0	0	1		3	6	37
	Sha^{Sha}	10	2	1	1		2	40
	Ws-4$^{Ws\text{-}4}$	4	3	0	0	4		37
	Ely^{Ely}	41	45	44	42	nd	42	

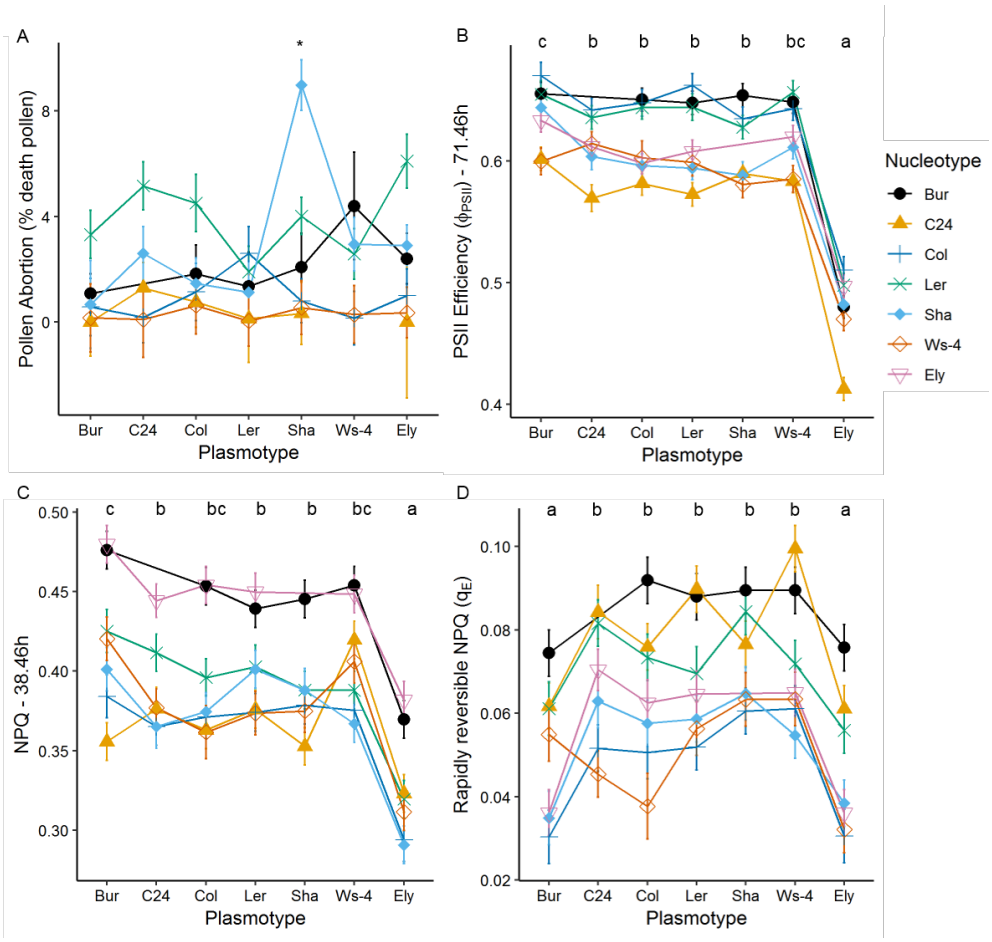

Figure 2. Plasmotype changes result in cytonuclear epistasis, and in the case of cybrids with the Ely and Bur plasmotype also in additive effects. A) Pollen abortion, percentage of dead pollen out of 250. B) PSII efficiency (Φ_{PSII}) 71.46 hours after start of experiment, after a full day of fluctuating light with a maximum difference between 500 and 100 µmol/m^2/s irradiance (see Fig. 3C for light treatment). C) NPQ at 38.46 hours after start of experiment, which is at 300 µmol/m^2/s on a sigmoidal light curve starting at 65 µmol/m^2/s. D) The rapidly reversible component of NPQ, q_E, at 259 µmol/m^2/s after a full day of fluctuating light with a maximum difference between 500 and 100µmol/m^2/s. X-axis are labelled with the plasmotype, and the colours represent the nucleotypes. Any deviation from a horizontal line represents a potential additive or epistatic effect. Error bars represent the standard error of the mean. The * in panel A indicates a unique significant difference between the Sha^{Sha} cybrid and other cybrids with Sha nucleotypes (epistasis) (Hochberg's test, n=4-10). The letters above panels B, C and D represent significant differences between plasmotypes regardless of the nucleotype (additivity) (Hochberg's test, n=4*7). For panels B, C and D plants were grown at 200 µmol/m^2/s for 21 days prior to starting the experiment.

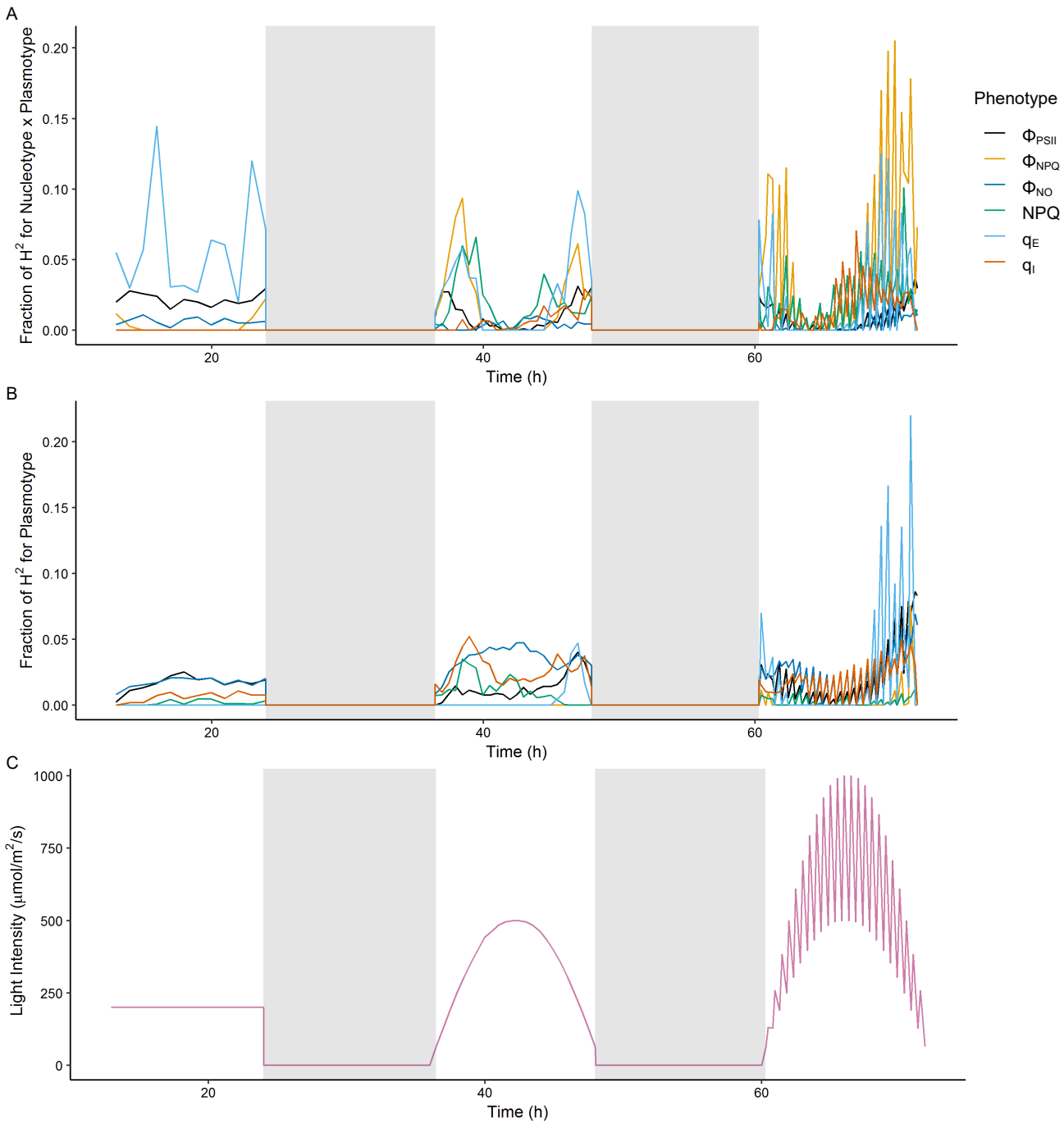

Figure 3. The fraction of explained genetic variation (H^2) for photosynthesis phenotypes differs depending on light conditions. A) shows the fraction of H^2 for plasmotype epistatic effects. B) shows the fraction of H^2 for plasmotype additive effects. C) shows the light intensity for three consecutive days with growth under steady light (day 1), sinusoidal light intensity (day 2) and fluctuating light intensity (day 3). Days are separated by nights (shaded areas). Note that the fraction of H^2 for different phenotypes changes markedly during days 2 and 3. Some phenotypes are explained largely by additive effects (i.e. q_E) while others by interaction (i.e. Φ_{NPQ}). A replication of this experiment is shown in Supplementary Fig. 8.

199 Though the average total explained variance due to the cytonuclear epistasis is only 5.2%, these
200 interactions can have strong effects for specific phenotypes or in specific cybrids. Explained variance
201 for some phenotypes can be markedly higher, for example for projected leaf area this amounts to 12.3%,
202 for hyponastic leaf movement to 8.3% and for ΦNPQ to 17.8%. A strong epistatic effect in pollen abortion
203 (43.5%) was due to relatively high pollen abortion in Sha^{Sha} (Fig. 2A) that we also observed in Sha
204 wildtype. The increased pollen abortion in its native nucleotype is surprising and could indicate either
205 incomplete compensation due to the accumulation of deleterious variants or perhaps to facilitate
206 increased outcrossing. The only cybrid for which we initially failed to obtain seed was Ely^{Sha}. This haploid
207 was regenerated and pollinated with wild-type Ely pollen to increase the chance of seed set. The diploid
208 offspring showed 45% of pollen abortion and were male sterile, indicating that in combination with the
209 Ely nucleotype the Sha plasmotype results in cytoplasmic male sterility (Supplementary Fig. 9). In
210 combination with the Sha plasmotype pollen abortion across the seven nucleotypes can range from near
211 zero, to 8.9% in Sha^{Sha} and to full male sterility in Ely^{Sha}, highlighting the strong epistasis that can be
212 present.

213 Cybrids with the Ely plasmotype exhibit clear additive effects: all have a lower PSII efficiency
214 (Φ_{PSII}) (Fig. 2B) and lower values for other photosynthesis related phenotypes i.e. NPQ, q_E and
215 chlorophyll content (Fig. 2C and Supplementary Data 2). This reduced Φ_{PSII} is likely to be responsible
216 for the concomitant reductions in biomass, growth rate and seed size and altered primary metabolite
217 content (Supplementary Data 2). To test whether additive effects could also be detected at the level of
218 gene expression we contrasted the transcriptome of Ely^{Ely} with that of the Ely^{Ler} and Ely^{Bur} cybrids. We
219 also compared the transcriptomes of Ler^{Ler}, Ler^{Bur}, *and* Ler^{Ely} (Supplementary Data 3; for details see
220 Supplementary Fig. 10 and Supplementary Table 5). Exchanging the Ely plasmotype with L*er* or Bur, in
221 either the L*er* or Ely nuclear background resulted in a consistent change in the expression of 40 genes,
222 of which most were upregulated (Supplementary Table 6). A GO-term analysis revealed that these
223 genes are significantly enriched for those involved in photorespiration (GO:0009853) and in glycine- and
224 serine family amino acid metabolism (GO:0006544 and GO:0009069) (Supplementary Data 3). This is
225 in line with the low serine and glycine content of cybrids with the Ely plasmotype which suggests reduced
226 photorespiration (Supplementary Data 2) (Somerville and Ogren, 1980) and can be linked to lower
227 overall photosynthetic activity.

228 The Ely plasmotype was deliberately included in our panel for its strong additive effect. In
229 addition to Ely we also observed strong additive effects from the Bur plasmotype which are mainly
230 restricted to the photosynthetic parameters. Under normal conditions PSII efficiency is slightly increased
231 by the Bur plasmotype (1.6%), however when fluctuating the light intensity, this difference becomes
232 more apparent (3.5% increase) (Fig. 2B and 3). This increase in Φ_{PSII}, under fluctuating conditions
233 results in a corresponding reduction in Φ_{NO} and Φ_{NPQ} of 7.3% and 2.2% respectively. NPQ, q_E and q_I
234 are also influenced by the plasmotype, but the time points at which these differences occur differs per
235 phenotype (Fig. 3A and B). The Bur plasmotype increases NPQ, with the largest increase of 5.9% at
236 the beginning of day 2 (38.46h) (Fig. 2C), while the rapidly reversible component of NPQ, q_E, has a
237 maximum reduction of 26.6% at the end of day 3 (71.46h) (Fig. 2D).

238 These photosynthesis-related phenotypes are likely to be due to chloroplast-derived variation.
239 In support of a chloroplastic origin for this photosynthetic variation, measurements of mitochondrial
240 respiration suggest that Bur is not an outlier and shows standard respiration rates (Supplementary Fig.
241 11). Based on coverage plots there are no obvious duplications or deletions in the mitochondrial or
242 chloroplast sequence of Bur thus we expect that altered expression or protein activity as opposed to
243 gene gain or loss is driving the Bur derived phenotypes (Supplementary Fig. 12). We annotated the
244 sequence variation of all plasmotypes using SnpEff (Cingolani et al., 2012). From this we found no large
245 effect mutations in the Bur mitochondria. There were, however, unique missense variants in the
246 chloroplastic genes MATURASE K (MATK), NAD(P)H-QUINONE OXIDOREDUCTASE SUBUNIT 6
247 (NDHG) and chloroplast open reading frame 1 (YCF1) as well as a frameshift mutation in tRNA-Lys
248 (TRNK) (Supplementary Data 4). NDHG is part of the NAD(P)H-dehydrogenase-like complex (NDH).
249 NDH is located inside the thylakoid membrane and acts, amongst others, as a proton pump in cyclic
250 electron flow around photosystem I and chlororespiration. NDH creates a pH differential that can be
251 causative of the observed non-photochemical quenching phenotypes (Strand et al., 2017; Laughlin et
252 al., 2019). In contrast to Ely, the plasmotype which evolved in response to the use of herbicides, an
253 anthropogenic selective pressure (Flood et al., 2016), the Bur plasmotype represents a naturally
254 occurring plasmotype that has an additive impact on key photosynthetic phenotypes.

255 Our experiments have shown that a clean, systematic exploration of plasmotypic variation in a
256 plant species is feasible. To our knowledge, apart from the *cenh3* mutant used here, there is only one
257 other intraspecific haploid inducer available (the maize *ig* mutant) which can be used via the maternal

258 line and thus replace the plasmotype (Kermicle, 1969; Schneerman et al., 2000; Houben et al., 2011).
259 Current knowledge of *cenh3* mediated uniparental genome elimination should allow for the creation of
260 maternal haploid inducers in a wider range of species (Karimi-Ashtiyani et al., 2015). This would allow
261 elite nucleotypes to be brought into new plasmotypic backgrounds to explore novel plasmotype-
262 nucleotype combinations. Our data indicate that there is substantial variation for phenotypes such as
263 NPQ and Φ_{PSII} which are important for plant productivity (Flood et al., 2011; Kromdijk et al., 2016;
264 Murchie et al., 2018). Next to Ely, we identified one new plasmotype (Bur) that significantly impacts
265 photosynthesis in an additive manner. Expanding our panel would likely find more, suggesting that future
266 research aiming to enhance crop photosynthesis should play close attention to available plasmotypic
267 variation. Apart from studying natural variation, the use of haploid inducers as plasmotype donors could
268 be used to transfer cytoplasmic male sterility (CMS), herbicide resistances or genetically engineered
269 plasmotypes. Plant plasmotypes, are notoriously difficult to genetically modify, although recently there
270 have been some advances in this regard (Jin and Daniell, 2015; Zhang et al., 2015; Kwak et al., 2019;
271 Ruf et al., 2019). The use of haploid inducers as plasmotype donors could further increase the
272 accessibility of such modifications as transformations could be undertaken in a compatible nucleotype
273 and once achieved can be transferred into different nucleotypes, thus amplifying the potential impact of
274 successful plasmotype modifications.

275 Exploring the potential of plasmotypic variation via the use of haploid inducer lines is not only
276 promising for plant breeding, but also for understanding the role such variation plays in plant adaptation
277 (Bock et al., 2014; Dobler et al., 2014). Our results show that despite considerable genetic divergence
278 between the genotypes used in our panel, all cybrids were viable, this in itself suggests a remarkable
279 degree of conservation for the fundamental components of cytonuclear interactions. Although we do
280 find clear additive effects of some plasmotypes, the majority of the plasmotype derived variation
281 manifests as epistasis in the traits we measured which is in line with previous research in plants, animals,
282 and fungi (Zeyl et al., 2005; Dowling et al., 2007; Montooth et al., 2010; Joseph et al., 2013; Roux et al.,
283 2016). Also in line with studies of mitonuclear interactions in animals is the observation that phenotypic
284 variation due to plasmotypic variation becomes more pronounced under fluctuating and stressful
285 conditions (Dowling et al., 2007; Hoekstra et al., 2013; Mossman et al., 2016; Hill et al., 2019). Both our
286 results and previous work suggests that multilevel interactions (i.e. Nucleotype x Plasmotype x
287 Environment) may be the primary mechanism by which plasmotypic variation is expressed. Thus,

288 plasmotypic variation may act as an evolutionary capacitor providing novel phenotypes in specific
289 genetic and environmental contexts, such variation may be particularly important for both crops and wild
290 species in our rapidly changing climate.
291

292 **Online methods**

293 *Plant materials:* Seven *Arabidopsis* accessions were chosen for the construction of a full nucleotype-
294 plasmotype diallel. Ely (CS28631) is atrazine resistant due to a chloroplast-encoded mutation in *PsbA*
295 which leads to a modified D2 protein that greatly reduces PSII efficiency (El-Lithy et al., 2005). Ws-4
296 (CS5390) was included for its unusual photosystem II phosphorylation dynamics (Yin et al., 2012). Bur
297 (CS76105) is commonly used in diversity panels and is a standard reference accession. Sha (CS76227)
298 was selected based on its capacity to induce cytoplasmic male sterility in some crosses (Gobron et al.,
299 2013). The set was completed by adding L*er* (CS76164), Col (CS76113) and C24 (CS76106) which are
300 three widely used genotypes in *Arabidopsis* research. Col is the reference genome for nuclear and
301 chloroplast sequences and C24 for the mitochondrial sequence. The *GFP-tailswap* haploid-inducer that
302 expresses a GFP-tagged CENTROMERE HISTONE 3 protein in a *cenh3/htr12* mutant background, is
303 in a Col background (Ravi and Chan, 2010).

304

305 *Generation of a nucleotype-plasmotype diallel*: To generate new nucleotype-plasmotype combinations,
306 plants of all seven accessions (Bur, C24, Col, Ely, L*er*, Sha and Ws-4) were crossed as males to *GFP-*
307 *tailswap* resulting in all cybrids with the Col plasmotype. New HI lines were created by crossing the
308 original *GFP-tailswap* line as a male to the six additional plasmotype mothers (Bur, C24, Ely, L*er*, Sha
309 and Ws-4). Genome elimination does not always occur and some of the offspring were diploid F1 lines.
310 These were selfed and F2 lines homozygous for the *cenh3/htr12* mutation and carrying the *GFP-*
311 *tailswap* were selected as new HI lines in different plasmotypic backgrounds (Fig. 1A). Plants of all
312 seven accessions were then crossed as males to these new HI lines and the haploids arising from these
313 49 crosses were identified based on their phenotype (as described in Wijnker et al. (2014)). These
314 haploid lines self-fertilized, either following somatic genome duplication or after restitutional meiosis
315 (Ravi and Chan, 2010), and gave rise to doubled haploid offspring (Fig. 1B). The resulting 49 lines
316 comprise a full diallel of 21 pairs of reciprocal nucleotype-plasmotype combinations (cybrids) as well as
317 seven nucleotype-plasmotype combinations that have, in principle, the same nucleotype-plasmotype
318 combinations as their wild-type progenitors (self-cybrids; Fig. 1C, diagonal). All cybrids and the wild-
319 type accessions were propagated for one generation before use in further experiments, with the
320 exception of Ely^{Sha} of which the original haploid died without setting seed and was recreated at a later
321 stage by generating haploids that were pollinated with Ely wild-type plants to ensure seed set.

322

323 *Genotype confirmation*: To confirm that all cybrids in our panel are authentic, all 49 cybrids and 7 wild-
324 type progenitors were whole-genome sequenced at the Max Planck Genome Centre Cologne
325 (Germany) using Illumina Hiseq 2500 150-bp paired-end sequencing. The cybrids were sequenced at
326 8.5X coverage and the wild-type progenitors at 40X coverage. To remove erroneous bases, we
327 performed adapter and quality trimming using Cutadapt (version 1.18) (Martin, 2011). Sequences were
328 clipped if they matched at least 90% of the total length of one of the adapter sequences provided in the
329 NEBNext Multiplex Oligos for Illumina® (Index Primers Set 1) instruction manual. In addition, we
330 trimmed bases from the 5' and 3' ends of reads if they had a phred score of 20 or lower. Reads that
331 were shorter than 70 bp after trimming were discarded. Trimmed reads were aligned to a modified
332 version of the A. thaliana Col-0 reference genome (TAIR10, European Nucleotide Accession number:
333 GCA_000001735.2) which contains an improved assembly of the mitochondrial sequence (Genbank
334 accession number: BK010421) (Sloan et al., 2018) using bwa mem (version 0.7.10-r789) (Li, 2013) with
335 default parameters. The resulting alignment files were sorted and indexed using samtools (version 1.3.1)
336 (Li et al., 2009). Duplicate read pairs were marked using the MarkDuplicates tool of the GATK suite
337 (version 4.0.2.1), using an optical duplicate pixel distance of 100, as recommended in the documentation
338 of GATK when working with data from unpatterned Illumina flowcells. Variants were called using a
339 workflow based on GATK Best Practices. Base quality scores of aligned reads were recalibrated using
340 GATK BaseRecalibrator with default parameters, using a set of variants of a world-wide panel of 1135
341 *A. thaliana* accessions (The 1001 Genomes Consortium, 2016) (obtained from
342 ftp://ftp.ensemblgenomes.org/pub/plants/release-37/vcf/arabidopsis_thaliana/) as known sites.
343 Following base recalibration, variants were called in each sample using GATK HaplotypeCaller, allowing
344 for a maximum of three alternate alleles at each site. Samples were then jointly genotyped using GATK
345 GenomicsDBImport and GATK GenotypeGVCFs with default parameters. This last step generated three
346 different VCF files: one containing the calls of the nuclear genome, one containing calls of the
347 mitochondrial genome and one containing calls of the chloroplast genome.

348 To remove likely false positive calls, we filtered the callsets using two complementary
349 approaches. First, we filtered the nuclear callset using GATK VariantRecalibrator and GATK
350 ApplyVQSR (--truth-sensitivity-filter-level set at 99.9), using the set of variants called in the world-wide
351 panel of 1135 A. thaliana accessions as a training and truth set (prior=10.0). This step could not be

352 performed for the mitochondrial and chloroplast calls, as these lack a golden truth set that can be used
353 for recalibration. Second, we filtered variants based on their quality by depth score (QD). For the nuclear
354 callset, we used a QD score of 40, leaving 3.7 million SNPs, for the chloroplast callset a QD of 25,
355 leaving 356 SNPs and for the mitochondrial callset a QD of 20, leaving 135 SNPs.

356 46 cybrids were found to have the correct genotypes. With one line, Bur^{Ws-4}, there was a sample
357 mix-up during library preparation with Sha^{Sha}. Leading to two Sha^{Sha} samples and no sequenced Bur^{Ws-}
358 ^{4} sample. Fortunately, we did have a true Bur^{Ws-4} cybrid, which we confirmed via both phenotype (Bur
359 and Sha nucleotypes are phenotypically distinct from one another) and genotype through the KASP^{TM}
360 markers (see below) (Supplementary Table 8). To confirm the Sha cybrids we therefore used the Sha
361 genotype (CS76382) from the 1001 genomes project (The 1001 Genomes Consortium, 2016). Two
362 other lines, $C24^{C24}$ and $Ws\text{-}4^{Col}$, had a high number of heterozygous calls in their plasmotypes, with
363 $C24^{C24}$ being heterozygous with $C24^{Col}$ and $Ws\text{-}4^{Col}$ being heterozygous with $Ws\text{-}4^{Bur}$. As in the
364 production of $Ws\text{-}4^{Col}$ no plant was used with a Bur plasmotype, this cannot be heteroplasmy. To ensure
365 that this was a sample mix-up and the putative event of cross-contamination had occurred in the
366 laboratory, we designed KASP^{TM} makers (LGC, https://www.lgcgroup.com) and genotyped all lines.
367 These KASP^{TM} markers are designed to be unique to the chloroplast of one accession, and designed
368 on SNPs that were called heterozygous in the sequence analysis (Supplementary Table 7). The KASP^{TM}
369 assay can distinguish between both homozygouse or heterozygous states. We ran all seven KASP^{TM}
370 markers on all lines, for $C24^{C24}$ and $Ws\text{-}4^{Col}$ this included plants from the same seed batch as the plants
371 used for sequencing, as well as direct offspring of the sequenced plants. All lines showed the correct
372 genotypes, and no heterozygosity was observed in any of the lines, including $C24^{C24}$ and $Ws\text{-}4^{Col}$
373 (Supplementary Table 8). Unfortunately, the Ely^{Sha} used for sequencing died before setting seed and
374 although it has since been recreated, it could not be included in our phenotypic analyses. We have used
375 the KASP^{TM} marker for the Sha chloroplast, and confirmed it to be correct (Supplementary Table 8).

376 To check for any incomplete chromosome elimination, we calculated the read coverage for all
377 cybrids, normalized per chromosome. We did not observe any remaining chromosomes, although we
378 found a 200kb duplication of nuclear DNA in Bur^{Bur} and Bur^{C24}. In Bur^{C24} and the self-cybrid Bur^{Bur} we
379 discovered the presence of a duplicated segment on chromosome 2. Because this duplicated segment
380 is present (and identical) in two independent cybrid lines and this segment is of a Bur nuclear origin (i.e.
381 there are only Bur SNPs in this region), we conclude this segment results from a *de-novo* duplication in

382 one of the wild-type Bur lines used to generate these cybrids. Following the exclusion of phenotyping
383 data for Bur^{Bur} and Bur^{C24} we limited our analyses to 46 rather than 49 cybrids. The parental lines were
384 included in the screens to test for possible unforeseen effects of cybrid production (which involves a
385 haploid growth stage). This brings the number of phenotyped lines in this study to a total of 53 (40
386 cybrids, 6 self-cybrids and 7 wild types).

387 The fuctional effects of the chlorplastic and mitochondrial SNPs and INDELs were predicted
388 using SnpEff (Cingolani et al., 2012). A SnpEff database was built using the genome, transcriptome and
389 proteome as released in TAIR10.1. SNPs and INDELs were predicted on the filtered VCF, as mentioned
390 above. In the analysis we only considered varaints with a "HIGH" or "MODERATE" impact.

391

392 *Phenotyping*: Cybrids were phenotypically assessed using different platforms. For details on the number
393 of phenotypes per experiment see Supplementary Table 4.

394 Growth, PSII efficiency (Φ_{PSII}), chlorophyll reflectance and leaf movement (all parameters at
395 n=24) was screened in the Phenovator platform, a high-throughput phenotyping facility located in a
396 climate-controlled growth chamber (Flood et al., 2016). This phenotyping platform measured the plants
397 for: Φ_{PSII} using chlorophyll fluorescence, reflectance at 480 nm, 532 nm, 550 nm, 570 nm, 660 nm, 700
398 nm, 750 nm and 790 nm, and projected leaf area (PLA) based on pixel counts of near infra-red (NIR)
399 images (Flood et al., 2016). The growth chamber was set to a 10 h day/14 h night regime, at 20°C day
400 and 18°C night temperature, 200 µmol m^{-2} s^{-1} irradiance, and 70% relative humidity. The plants were
401 grown on a rockwool substrate and irrigated daily with a nutrient solution as described in Flood et al.
402 (2016).

403 Growth (n=24) and subsequently above ground biomass (n=12) was measured in another high-
404 throughput phenotyping facility (Kokorian et al., 2010), where projected leaf area was measured three
405 times per day with 14 fixed cameras (uEye Camera, IDS Imaging Development Systems GmbH,
406 Obersulm, Germany). This growth chamber was set to a 10 h day/14 h night regime, at 20°C day and
407 14°C night temperature, 200 µmol m^{-2} s^{-1} light and 70% relative humidity. Plants were grown on rockwool
408 and irrigated weekly with a nutrient solution as described before.

409 Non-fluctuating and fluctuating light treatments were performed in the DEPI phenotyping facility
410 of Michigan State University (n=4)(Cruz et al., 2016). This facility is able to measure the chlorophyll
411 fluorescence derived photosynthetic parameters, Φ_{PSII}, Φ_{NO}, Φ_{NPQ}, NPQ, q_E, q_I. Three-week-old plants

412 were moved into the facility, where they were left to acclimatize for 24 hours after which three days of
413 phenotyping was performed under different light regimes. On the first day the plants were illuminated
414 with a constant light intensity of 200 µmol m^{-2} s^{-1}. On the second day the plants received a sinusoidal
415 light treatment where the light intensity began low and gradually increased to a maximum of 500 µmol
416 m^{-2} s^{-1} light from which it deceased back down to 0. On the third day the plants received a fluctuating
417 light treatment ranging between 0 and 1000 µmol m^{-2} s^{-1} light in short intervals (Fig. 3C). For the second
418 experiment in the DEPI phenotyping facility the experiment was extent with 2 days, in which day 4
419 replicated day 2 and day 5 replicated day 2 (Supplementary Data 1 and Supplementary Fig. 8C). For
420 further details see Cruz et al. (2016).

421 Bolting time and flowering time were measured on all cybrids (n=10) in a greenhouse
422 experiment in April 2017, with the exception of Ely nucleotype cybrids which needed vernalisation and
423 were not included in this experiment. Additional lighting was turned on when the natural light intensity
424 fell below 685.5 µmol m^{-2} s^{-1}, and turned off when the light intensity reached 1142.5 µmol m^{-2} s^{-1}, with a
425 maximum of 16 h per day.

426 Seeds for the germination experiments were generated from two rounds of propagation. In the
427 first-round seeds were first sown in a growth chamber set to a 10 h day/14 h night regime, at 20°C day
428 and 18°C night temperature. 200 µmol$m^{-2}s^{-1}$ light intensity, and 70% relative humidity. After three weeks
429 they were moved to an illuminated cold room at 4°C for six weeks of vernalization. After vernalization
430 all plants (n=8) were moved to a temperature-controlled greenhouse (20°C) for flowering and seed
431 ripening. Exceptions to this were L*er*^{Ely}, L*er*$^{Ws-4}$, and Ely^{Ws-4} for which no doubled haploid seed was
432 available at the beginning of the first propagation round. L*er*^{Ely} and L*er*$^{Ws-4}$ were sown later, during the
433 vernalization stage and flowered at the same time as the vernalized plants. Ely^{Ws-4} produced haploid
434 seed at a later stage and could not be included in the first propagation round. Plants were grown in a
435 temperature-controlled greenhouse set at 20°C. In this round only lines with the Ely nucleotype were
436 vernalized. For the germination experiments seeds were stratified on wet filter paper for four days at
437 4°C before being assayed in the Germinator platform (Joosen et al., 2010) for seed size, germination
438 rate and total germination percentage. Germination under osmotic stress was performed on filter paper
439 with 125 mM NaCl. For the controlled deterioration treatment, seeds were incubated for 2.5, 5 or 7 days
440 at 40°C and 82% RH and subsequently assayed in the Germinator platform without stratification.

441 To assess pollen abortion all cybrid lines and wild-type progenitors (except those with the Ely
442 nucleotype) were grown simultaneously in a growth chamber (Percival) under controlled conditions
443 (16H/ 8H light cycle, 21º/18º ºC and 50%-60% relative humidity). Pollen abortion was manually
444 assessed for all the ecotypes by using a differential staining of aborted and non-aborted pollen grains
445 (Peterson et al., 2010). A total of three plants and three flowers per plant of each cybrid were collected
446 on the same day and submerged in a drop of 13 ul of phenol-free Alexander staining solution placed
447 on a glass slide with a glass cover slip of 18x18 mm. For each flower 250 pollen grains were counted
448 and the number of aborted pollen therein.
449 Oxygen consumption of seedlings was measured in 2 mL of deionized water with a liquid-
450 phase Oxytherm oxygen electrode system (Hansatech Instruments) calibrated at the measurement
451 temperature. Three-day-old seedlings (about 50 mg) were directly imbibed in the electrode chamber.
452 The rates of oxygen consumption were measured after tissue addition and subtracted from the rates
453 after addition of 500 µM KCN. Results are the mean of at least five measurements. Measurements for
454 different genotypes were performed on consecutive days, and to correct for daily variation, normalized
455 to Col-0 samples that were run daily.
456
457 *Metabolomics*: Plant material for primary metabolite analysis was obtained from the 'Phenovator'
458 photosynthetic phenotyping experiment. Plants were harvested 26 days after sowing, which due to the
459 10-hr photoperiod was prior to bolting for all lines. Samples were frozen in liquid nitrogen, and samples
460 of each genotype were subsequently combined into four pools each made up of material of
461 approximately six replicates. Each pool was ground and homogenized before an aliquot was taken for
462 further analysis. Reference samples for the metabolite analysis were composed of material from all
463 seven parents in equal amounts and then homogenized. The method used for the extraction of polar
464 metabolites from *Arabidopsis* leaves was adapted from Lisec et al. (2006) as described by Carreno-
465 Quintero et al. (2012). Specific adjustments for *Arabidopsis* samples were made as follows; the polar
466 metabolite fractions were extracted from 100 mg of *Arabidopsis* leaf material (fresh weight, with max.
467 5% deviation). After the extraction procedure, 100 µL aliquots of the polar phase were dried by vacuum
468 centrifugation for 16 hours. The derivatization was performed on-line similar as described by Lisec et al.
469 (2006) and the derivatized samples were analyzed by a GC-ToF-MS system composed of an Optic 3
470 high-performance injector (ATAS^{TM}, GL Sciences, Eindhoven, The Netherlands) and an Agilent 6890

471 gas chromatograph (Agilent Technologies, Santa Clara, California, United States) coupled to a Pegasus
472 III time-of-flight mass spectrometer (Leco Instruments, St. Joseph, Michigan, United States). Two
473 microliters of each sample were introduced in the injector at 70°C using 5% of the sample (split 20). The
474 detector voltage was set to 1750 Volts. All samples were analyzed in random order in four separate
475 batches. The systematic variation that inadvertently is introduced by working in batches, was removed
476 upon analysis of covariance. In this model the batch number was used as a factor (four levels) and "run
477 number within a batch" as a covariate since it is also expected that (some) variation will be introduced
478 by the sample run order within each batch. For this the S2 method described by (Wehrens et al., 2016)
479 was used to perform the least-squares regression. After quality control and removing metabolites with
480 more than 20% missing data and a broad sense heritability (H^2) of less than 5%, we were left with data
481 on 41 primary metabolites. Metabolites were identified based on the Level of Identification Standard of
482 the Metabolomics Standards Initiative (Sumner et al., 2007).
483
484 *Transcriptome analysis*: Using the same material as described in the metabolome analysis, total RNA
485 was extracted from six cybrids, three in a L*er* and three in an Ely nuclear background: L*er*^{Ler} L*er*^{Ely}, L*er*^{Bur}
486 and Ely^{Ler} Ely^{Ely}, Ely^{Bur} with three replicates per genotype, totaling 18 plants. Library preparation was
487 done with a selection on 3' polyadenylated tails to preferentially include nuclear mRNA. Read alignment
488 was done using TopHat (Trapnell et al., 2009). Any chloroplast and mitochondrial genes remaining were
489 excluded from further analysis. The raw counts were normalized and analyzed using the DeSeq2
490 package in R (Love et al., 2014). Genes for which the expression levels were significantly different
491 between two cybrids were determined by comparing two genotypes using the contrast function of
492 DeSeq2. P-values were determined using the Wald test, and p-values were adjusted using the
493 Benjamini-Hochberg correction (α=0.05). GO enrichment analysis was done using default setting in
494 g:profiler (g:GOSt). The complete set of detected genes in each cybrid was used as a statistical
495 background in the analysis (Reimand et al., 2016).
496
497 *Phenotypic data analysis*: We used the self-cybrids as our baseline in phenotypic comparisons to control
498 for any possible effects of cybrid creation, with the exception of Bur^{Bur} which was replaced in all analysis
499 with Bur-WT. Raw data was directly analyzed except for time series data of growth and chlorophyll
500 reflectance which was preprocessed as follows. Time series data were fitted with a smooth spline using

the gam function from the mgcv package in R (Wood et al., 2016). The fitted B-spline was subsequently used to derive curve parameters. These include area under the curve, slope under mean, first, second (median) and third quartile, minimal and maximal slope, and the timepoint where the slope is maximum. These parameters allow us to quantify not only plant size and growth rate but also the dynamic properties of the growth curve, i.e. did growth occur early of late, or was it more uniform? In addition, we calculated relative growth rate per time point by dividing the growth rate, relative to the plant size (Flood et al., 2016). All raw parameters and derived parameters were analyzed by fitting either a linear mixed model or a linear model. The linear mixed model was used when a random correction parameter was present, when such random correction parameters were absent a linear model was used. The models were analyzed using the Restricted Maximum Likelihood (REML) procedure for each relevant phenotype using the lme4 package in R (Bates et al., 2015). As each experiment had a different design, several models were employed (Supplementary Table 4). The following model was generally used, in some instances random terms (underlined below) were added:

$$\underline{Y} = Nucleotype + Plasmotype + (Nucleotype * Plasmotype) + \underline{Block} + \underline{\varepsilon} \qquad (1)$$

For every model, normality and equal variances were checked. Next for every phenotypic parameter we calculated significant difference, for the plasmotype and interaction term of the model (equation 1). This was done by ANOVA in which Kenward-Roger approximation for degrees of freedom was used. As posthoc tests we used a two-sided Dunnett's test, where we tested whether a given cybrid was different from the self-cybrid control, within one nucleotype. Two side Hochberg's posthoc tests were used when all pairwise comparisons were tested within one nucleotype (to test for epistasis) and across all nucleotypes (to test for additivity). The significance threshold for all posthoc tests was set at α=0.05. The contribution of the nucleotype, plasmotype and the interaction between the two, was determined by estimating the variance components in mixed models containing the same terms as in model (1). However, the fixed terms were taken as random:

$$\underline{Y} = \underline{Nucleotype} + \underline{Plasmotype} + \underline{(Nucleotype * Plasmotype)} + \underline{Block} + \underline{\varepsilon},$$

530 Where the variance components were estimated by the VarCorr function from the lme4 package. Total
531 variance was calculated by summing all the variance components, after which the fraction explained
532 variance for every term in the model was calculated. The broad sense heritability, in our case equal to
533 repeatability (Falconer and Mackay, 1996), is determined by the three genetic components, i.e.
534 nucleotype, plasmotype and their interaction. The fraction of broad sense heritability explained by the
535 separate genetic components was calculated subsequently.

536 In total we measured 1859 phenotypes. After data processing, further analysis was only
537 conducted on phenotypes with a broad sense heritability higher than 5%, removing phenotypes that
538 were non-informative, leaving with 1782 phenotypes. Furthermore, to avoid biases in the results due to
539 overly correlated data when stating summary statistics, we further subset the remaining 1782
540 phenotypes (Supplementary Data 2). Using a threshold based purely on correlation would favor the
541 inclusion of variation largely driven by the nucleotype. Because the population is balanced, we therefore
542 subtracted the averages of the nucleotype values from the cybrid phenotype values, to reveal the
543 plasmotype effect per cybrid. From these we calculated the pearson correlations for all phenotypes. This
544 highlighted that the most uncorrelated phenotypes mainly stem from one experiment assessing
545 photosynthetic parameters under fluctuating light. The unbiased selection of a subset of phenotypes
546 would result in the omission of several phenotypic categories. To present a balanced overview of all
547 phenotypic categories we manually selected a subset comprising the following phenotypes. For time
548 series in which we scored for up to 25 days after germination, we selected the morning measurements
549 of day 8, 13, 18 and 23. The time series analysis of fluctuating light were measured for three (first
550 experiment, Fig. 3) and five days (replicate experiment; Supplementary Fig. 8) in a row, with each day
551 subjected to a different treatment. As these treatments reached their extremes in the middle and at end
552 of the day, and the results of replicate experiments were very similar, we selected time points in the
553 middle and at the end of the day of only the first experiment. For the different seed treatments we used
554 the germination time until 50% of the seeds germinated. In addition, we included biomass, leaf
555 movement, seed size, flowering time as single phenotypes and all 36 primary metabolites. This resulted
556 in 92 phenotypes, that are used for giving summary- and test statistics (for a correlation plot of these,
557 please see Supplementary Fig. 6). All data on the 1859 phenotypes, with summary- and test statistics
558 are available in Supplementary Data 1 and Supplementary Table 3.

The correlation between plasmotype additive and plasmotype epistatic effects was calculated both with and without the Ely plasmotype. For both additive and epistatic effects every significant change between plasmotypes, within one nucleotype background, was counted (Supplementary Data 2). The Pearson correlation coefficients and accompanying p-values were calculated using the ggpubr package in R.

567 **References:**

568 **Bates D, Mächler M, Bolker B, Walker S** (2015) Fitting linear mixed-effects models using lme4.
569 Journal of Statistical Software **67:** 48
570 **Bock DG, Andrew RL, Rieseberg LH** (2014) On the adaptive value of cytoplasmic genomes in plants.
571 Mol. Ecol. **23:** 4899-4911
572 **Carreno-Quintero N, Acharjee A, Maliepaard C, Bachem CWB, Mumm R, Bouwmeester H, Visser**
573 **RGF, Keurentjes JJB** (2012) Untargeted Metabolic Quantitative Trait Loci Analyses Reveal a
574 Relationship between Primary Metabolism and Potato Tuber Quality. Plant Physiology **158:**
575 1306-1318
576 **Chan KX, Phua SY, Crisp P, McQuinn R, Pogson BJ** (2016) Learning the Languages of the Chloroplast:
577 Retrograde Signaling and Beyond. **67:** 25-53
578 **Cingolani P, Platts A, Wang LL, Coon M, Nguyen T, Wang L, Land SJ, Lu X, Ruden DM** (2012) A
579 program for annotating and predicting the effects of single nucleotide polymorphisms,
580 SnpEff. Fly **6:** 80-92
581 **Cingolani P, Platts A, Wang LL, Coon M, Nguyen T, Wang L, Land SJ, Lu X, Ruden DM** (2012) A
582 program for annotating and predicting the effects of single nucleotide polymorphisms,
583 SnpEff: SNPs in the genome of Drosophila melanogaster strain w(1118); iso-2; iso-3. Fly **6:** 80-
584 92
585 **Cruz JA, Savage LJ, Zegarac R, Hall CC, Satoh-Cruz M, Davis GA, Kovac WK, Chen J, Kramer DM**
586 (2016) Dynamic Environmental Photosynthetic Imaging Reveals Emergent Phenotypes. Cell
587 Systems **2:** 365-377
588 **Dobler R, Rogell B, Budar F, Dowling DK** (2014) A meta-analysis of the strength and nature of
589 cytoplasmic genetic effects. J. Evolution Biol. **27:** 2021-2034
590 **Dowling DK, Abiega KC, Arnqvist G** (2007) TEMPERATURE-SPECIFIC OUTCOMES OF CYTOPLASMIC-
591 NUCLEAR INTERACTIONS ON EGG-TO-ADULT DEVELOPMENT TIME IN SEED BEETLES. **61:** 194-
592 201
593 **El-Lithy ME, Rodrigues GC, van Rensen JJS, Snel JFH, Dassen HJHA, Koornneef M, Jansen MAK, Aarts**
594 **MGM, Vreugdenhil D** (2005) Altered photosynthetic performance of a natural *Arabidopsis*
595 accession is associated with atrazine resistance. J. Exp. Bot. **56:** 1625-1634
596 **Falconer D, Mackay TJH, Essex, UK: Longmans Green** (1996) Introduction to quantitative genetics.
597 1996. **3**
598 **Flood PJ, Harbinson J, Aarts MGM** (2011) Natural genetic variation in plant photosynthesis. Trends
599 Plant Sci. **16:** 327-335
600 **Flood PJ, Kruijer W, Schnabel SK, Schoor R, Jalink H, Snel JFH, Harbinson J, Aarts MGM** (2016)
601 Phenomics for photosynthesis, growth and reflectance in Arabidopsis thaliana reveals
602 circadian and long-term fluctuations in heritability. Plant Methods **12:** 1-14
603 **Flood Pádraic J, van Heerwaarden J, Becker F, de Snoo CB, Harbinson J, Aarts Mark GM** (2016)
604 Whole-Genome Hitchhiking on an Organelle Mutation. Current Biology **26:** 1306-1311
605 **Flood PJ, Yin L, Herdean A, Harbinson J, Aarts MGM, Spetea C** (2014) Natural variation in
606 phosphorylation of photosystem II proteins in Arabidopsis thaliana: is it caused by genetic
607 variation in the STN kinases? Philosophical Transactions of the Royal Society B: Biological
608 Sciences **369**
609 **Gobron N, Waszczak C, Simon M, Hiard S, Boivin S, Charif D, Ducamp A, Wenes E, Budar F** (2013) A
610 Cryptic Cytoplasmic Male Sterility Unveils a Possible Gynodioecious Past for *Arabidopsis*
611 *thaliana*. PLoS ONE **8:** e62450
612 **Hill GE, Havird JC, Sloan DB, Burton RS, Greening C, Dowling DK** (2019) Assessing the fitness
613 consequences of mitonuclear interactions in natural populations. **94:** 1089-1104
614 **Hoekstra LA, Siddiq MA, Montooth KL** (2013) Pleiotropic Effects of a Mitochondrial–Nuclear
615 Incompatibility Depend upon the Accelerating Effect of Temperature in
616 Drosophila. **195:** 1129-1139

Houben A, Sanei M, Pickering R (2011) Barley doubled-haploid production by uniparental chromosome elimination. **104:** 321-327

Jin S, Daniell H (2015) The Engineered Chloroplast Genome Just Got Smarter. Trends in Plant Science **20:** 622-640

Joosen RVL, Kodde J, Willems LAJ, Ligterink W, van der Plas LHW, Hilhorst HWM (2010) germinator: a software package for high-throughput scoring and curve fitting of Arabidopsis seed germination. The Plant Journal **62:** 148-159

Joseph B, Corwin JA, Li B, Atwell S, Kliebenstein DJ (2013) Cytoplasmic genetic variation and extensive cytonuclear interactions influence natural variation in the metabolome. eLife **2:** e00776

Joseph B, Corwin JA, Li B, Atwell S, Kliebenstein DJ (2013) Cytoplasmic genetic variation and extensive cytonuclear interactions influence natural variation in the metabolome, Vol 2

Joseph B, Corwin JA, Züst T, Li B, Iravani M, Schaepman-Strub G, Turnbull LA, Kliebenstein DJ (2013) Hierarchical Nuclear and Cytoplasmic Genetic Architectures for Plant Growth and Defense within Arabidopsis. The Plant Cell Online **25:** 1929-1945

Karimi-Ashtiyani R, Ishii T, Niessen M, Stein N, Heckmann S, Gurushidze M, Banaei-Moghaddam AM, Fuchs J, Schubert V, Koch K, Weiss O, Demidov D, Schmidt K, Kumlehn J, Houben A (2015) Point mutation impairs centromeric CENH3 loading and induces haploid plants. **112:** 11211-11216

Kermicle JL (1969) Androgenesis Conditioned by a Mutation in Maize. **166:** 1422-1424

Kleine T, Leister D (2016) Retrograde signaling: Organelles go networking. Biochimica et Biophysica Acta (BBA) - Bioenergetics **1857:** 1313-1325

Kokorian J, Polder G, Keurentjes JJB, Vreugdenhil D, Olortegui Guzman MC (2010) An ImageJ based measurement setup for automated phenotyping of plants. *In* A Jahnen, C Moll, eds, Proceedings of the ImageJ User and Developer Conference, Luxembourg, Luxembourg, 27-29 October 2010. Centre de Recherche Public Henri Tudor, Luxembourg, pp 178-182

Kromdijk J, Głowacka K, Leonelli L, Gabilly ST, Iwai M, Niyogi KK, Long SP (2016) Improving photosynthesis and crop productivity by accelerating recovery from photoprotection. Science **354:** 857-861

Kwak S-Y, Lew TTS, Sweeney CJ, Koman VB, Wong MH, Bohmert-Tatarev K, Snell KD, Seo JS, Chua N-H, Strano MS (2019) Chloroplast-selective gene delivery and expression in planta using chitosan-complexed single-walled carbon nanotube carriers. Nature Nanotechnology **14:** 447-455

Levings CS (1990) The Texas Cytoplasm of Maize: Cytoplasmic Male Sterility and Disease Susceptibility. Science **250:** 942-947

Li H (2013) Aligning sequence reads, clone sequences and assembly contigs with BWA-MEM. *In* arXiv e-prints,

Li H, Handsaker B, Wysoker A, Fennell T, Ruan J, Homer N, Marth G, Abecasis G, Durbin R, Subgroup GPDP (2009) The Sequence Alignment/Map format and SAMtools. Bioinformatics **25:** 2078-2079

Lisec J, Schauer N, Kopka J, Willmitzer L, Fernie AR (2006) Gas chromatography mass spectrometry-based metabolite profiling in plants. Nat. Protocols **1:** 387-396

Love MI, Huber W, Anders S (2014) Moderated estimation of fold change and dispersion for RNA-seq data with DESeq2. Genome Biology **15:** 550

Martin M (2011) Cutadapt removes adapter sequences from high-throughput sequencing reads. 2011 **17:** 3 %J EMBnet.journal

Miclaus M, Balacescu O, Has I, Balacescu L, Has V, Suteu D, Neuenschwander S, Keller I, Bruggmann R (2016) Maize Cytolines Unmask Key Nuclear Genes That Are under the Control of Retrograde Signaling Pathways in Plants. Genome Biology and Evolution **8:** 3256-3270

Montooth KL, Meiklejohn CD, Abt DN, Rand DM (2010) MITOCHONDRIAL–NUCLEAR EPISTASIS AFFECTS FITNESS WITHIN SPECIES BUT DOES NOT CONTRIBUTE TO FIXED INCOMPATIBILITIES BETWEEN SPECIES OF DROSOPHILA. Evolution **64:** 3364-3379

Mossman JA, Biancani LM, Zhu C-T, Rand DM (2016) Mitonuclear Epistasis for Development Time and Its Modification by Diet in Drosophila. **203:** 463-484

Mossman JA, Ge JY, Navarro F, Rand DM (2019) Mitochondrial DNA Fitness Depends on Nuclear Genetic Background in Drosophila. **9:** 1175-1188

Murchie EH, Kefauver S, Araus JL, Muller O, Rascher U, Flood PJ, Lawson T (2018) Measuring the dynamic photosynthome. Annals of Botany **122:** 207-220

Peterson R, Slovin JP, Chen CJIJoPB (2010) A simplified method for differential staining of aborted and non-aborted pollen grains. **1:** e13-e13

Petrillo E, Godoy Herz MA, Fuchs A, Reifer D, Fuller J, Yanovsky MJ, Simpson C, Brown JWS, Barta A, Kalyna M, Kornblihtt AR (2014) A Chloroplast Retrograde Signal Regulates Nuclear Alternative Splicing. Science **344:** 427-430

Ravi M, Chan SWL (2010) Haploid plants produced by centromere-mediated genome elimination. **464:** 615-618

Ravi M, Marimuthu MPA, Tan EH, Maheshwari S, Henry IM, Marin-Rodriguez B, Urtecho G, Tan J, Thornhill K, Zhu F, Panoli A, Sundaresan V, Britt AB, Comai L, Chan SWL (2014) A haploid genetics toolbox for Arabidopsis thaliana. Nat Commun **5**

Reimand J, Arak T, Adler P, Kolberg L, Reisberg S, Peterson H, Vilo J (2016) g:Profiler—a web server for functional interpretation of gene lists (2016 update). Nucleic Acids Research **44:** W83-W89

Roux F, Mary-Huard T, Barillot E, Wenes E, Botran L, Durand S, Villoutreix R, Martin-Magniette M-L, Camilleri C, Budar F (2016) Cytonuclear interactions affect adaptive traits of the annual plant *Arabidopsis thaliana* in the field. Proceedings of the National Academy of Sciences **113:** 3687-3692

Ruf S, Forner J, Hasse C, Kroop X, Seeger S, Schollbach L, Schadach A, Bock R (2019) High-efficiency generation of fertile transplastomic Arabidopsis plants. Nature Plants **5:** 282-289

Sambatti JBM, Ortiz-Barrientos D, Baack EJ, Rieseberg LH (2008) Ecological selection maintains cytonuclear incompatibilities in hybridizing sunflowers. **11:** 1082-1091

Schneerman M, Charbonneau M, Weber DJMGCN (2000) A survey of ig containing materials. 54-55

Sloan DB, Wu Z, Sharbrough J (2018) Correction of Persistent Errors in Arabidopsis Reference Mitochondrial Genomes. **30:** 525-527

Somerville CR, Ogren WL (1980) Photorespiration mutants of *Arabidopsis thaliana* deficient in serine-glyoxylate aminotransferase activity. Proceedings of the National Academy of Sciences **77:** 2684-2687

Sumner LW, Amberg A, Barrett D, Beale MH, Beger R, Daykin CA, Fan TW-M, Fiehn O, Goodacre R, Griffin JL, Hankemeier T, Hardy N, Harnly J, Higashi R, Kopka J, Lane AN, Lindon JC, Marriott P, Nicholls AW, Reily MD, Thaden JJ, Viant MR (2007) Proposed minimum reporting standards for chemical analysis. Metabolomics **3:** 211-221

Tang Z, Hu W, Huang J, Lu X, Yang Z, Lei S, Zhang Y, Xu C (2014) Potential Involvement of Maternal Cytoplasm in the Regulation of Flowering Time via Interaction with Nuclear Genes in Maize. Crop Sci. **54:** 544-553

The 1001 Genomes Consortium (2016) 1,135 Genomes Reveal the Global Pattern of Polymorphism in Arabidopsis thaliana. Cell

Trapnell C, Pachter L, Salzberg SL (2009) TopHat: discovering splice junctions with RNA-Seq. Bioinformatics **25:** 1105-1111

Wehrens R, Hageman JA, van Eeuwijk F, Kooke R, Flood PJ, Wijnker E, Keurentjes JJB, Lommen A, van Eekelen HDLM, Hall RD, Mumm R, de Vos RCH (2016) Improved batch correction in untargeted MS-based metabolomics. Metabolomics **12:** 88

Wijnker E, Deurhof L, van de Belt J, de Snoo CB, Blankestijn H, Becker F, Ravi M, Chan SWL, van Dun K, Lelivelt CLC, de Jong H, Dirks R, Keurentjes JJB (2014) Hybrid recreation by reverse breeding in Arabidopsis thaliana. Nature protocols **9:** 761-772

Wood SN, Pya N, Säfken B (2016) Smoothing Parameter and Model Selection for General Smooth Models. Journal of the American Statistical Association **111:** 1548-1563

721 **Yin L, Fristedt R, Herdean A, Solymosi K, Bertrand M, Andersson MX, Mamedov F, Vener AV,**
722 **Schoefs B, Spetea C** (2012) Photosystem II Function and Dynamics in Three Widely Used
723 *Arabidopsis thaliana* Accessions. PLoS ONE **7:** e46206
724 **Zeyl C, Andreson B, Weninck E** (2005) NUCLEAR-MITOCHONDRIAL EPISTASIS FOR FITNESS IN
725 SACCHAROMYCES CEREVISIAE. Evolution **59:** 910-914
726 **Zhang J, Khan SA, Hasse C, Ruf S, Heckel DG, Bock R** (2015) Full crop protection from an insect pest
727 by expression of long double-stranded RNAs in plastids. Science **347:** 991-994

728

729

Acknowledgements: Hetty Blankestijn, Jose van de Belt, Daniel Oberste-Lehn, Elio Schijlen, Corrie Hanhart, and Joris ter Riele (all Wageningen University & Research) are acknowledged for help with experiments, Jonas Klasen (Max Planck Institute for Plant Breeding Research) for statistical advice, and Duur Aanen (Wageningen University & Research) for helpful discussions.

Author contributions: P.J.F. and E.W. conceived and designed the study. T.P.J.M.T. designed and performed the statistical analysis with help from P.J.F., W.K. and F.v.E.. P.J.F., T.P.J.M.T., E.K., F.F.M.B., L.W., V.C.B., J.v.A., J.M.G., and L.S. performed experiments. P.J.F., T.P.J.M.T., K.S., P.K., E.S., J.A.H., S.K.S., R.W., W.L., R.M., F.v.E. and E.W. analysed data. D.M.K., J.J.B.K., M.K., J.H. and M.G.M.A. contributed to the interpretation of results. P.J.F., T.P.J.M.T. and E.W. wrote the paper with significant contributions from M.K., J.H. and M.G.M.A. All authors read and approved the final manuscript.

Competing interests statement: The authors declare no competing interests

Data availability: Sequencing and transcriptome data will be available in the European Nucleotide Archive with the primary accession code PRJEB29654. The raw datasets will be made available through Dryad, a reporting summary will be provided. The analysed datasets that support our findings are available as supplementary datasets. The associated raw data for Fig. 2 and 3 are provided in Supplementary Data 1, the raw data for Table 1 is provided in Supplementary Data 2. The germplasm generated in this project will be available via NASC.